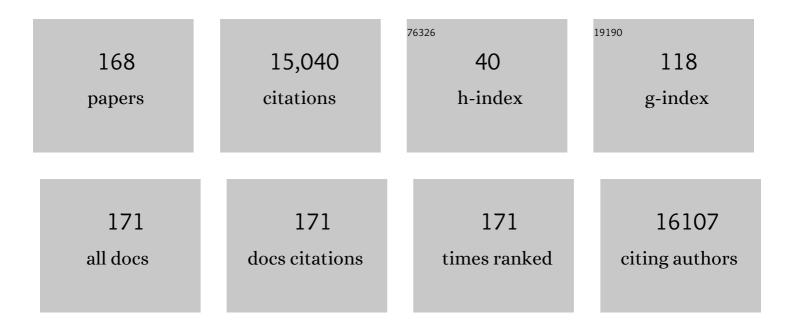
## Max A Viergever

List of Publications by Year in descending order

Source: https://exaly.com/author-pdf/8417400/publications.pdf Version: 2024-02-01



#	Article	lF	CITATIONS
1	elastix: A Toolbox for Intensity-Based Medical Image Registration. IEEE Transactions on Medical Imaging, 2010, 29, 196-205.	8.9	3,159
2	A survey of medical image registration. Medical Image Analysis, 1998, 2, 1-36.	11.6	2,486
3	Mutual-information-based registration of medical images: a survey. IEEE Transactions on Medical Imaging, 2003, 22, 986-1004.	8.9	2,311
4	A deep learning framework for unsupervised affine and deformable image registration. Medical Image Analysis, 2019, 52, 128-143.	11.6	512
5	Assessment of algorithms for mitosis detection in breast cancer histopathology images. Medical Image Analysis, 2015, 20, 237-248.	11.6	338
6	Adaptive Stochastic Gradient Descent Optimisation for Image Registration. International Journal of Computer Vision, 2009, 81, 227-239.	15.6	336
7	Explainable artificial intelligence (XAI) in deep learning-based medical image analysis. Medical Image Analysis, 2022, 79, 102470.	11.6	256
8	End-to-End Unsupervised Deformable Image Registration with a Convolutional Neural Network. Lecture Notes in Computer Science, 2017, , 204-212.	1.3	251
9	Automatic coronary artery calcium scoring in cardiac CT angiography using paired convolutional neural networks. Medical Image Analysis, 2016, 34, 123-136.	11.6	228
10	A survey of medical image registration – under review. Medical Image Analysis, 2016, 33, 140-144.	11.6	224
11	MRBrainS Challenge: Online Evaluation Framework for Brain Image Segmentation in 3T MRI Scans. Computational Intelligence and Neuroscience, 2015, 2015, 1-16.	1.7	179
12	Automatic Calcium Scoring in Low-Dose Chest CT Using Deep Neural Networks With Dilated Convolutions. IEEE Transactions on Medical Imaging, 2018, 37, 615-625.	8.9	176
13	A Recurrent CNN for Automatic Detection and Classification of Coronary Artery Plaque and Stenosis in Coronary CT Angiography. IEEE Transactions on Medical Imaging, 2019, 38, 1588-1598.	8.9	172
14	Deep Learning for Multi-task Medical Image Segmentation in Multiple Modalities. Lecture Notes in Computer Science, 2016, , 478-486.	1.3	165
15	Recursive calibration of the fiber response function for spherical deconvolution of diffusion MRI data. Neurolmage, 2014, 86, 67-80.	4.2	163
16	Deep learning analysis of the myocardium in coronary CT angiography for identification of patients with functionally significant coronary artery stenosis. Medical Image Analysis, 2018, 44, 72-85.	11.6	154
17	Deep Learning for Automatic Calcium Scoring in CT: Validation Using Multiple Cardiac CT and Chest CT Protocols. Radiology, 2020, 295, 66-79.	7.3	140
18	Coronary artery centerline extraction in cardiac CT angiography using a CNN-based orientation classifier. Medical Image Analysis, 2019, 51, 46-60.	11.6	129

#	Article	IF	CITATIONS
19	Standardized food images: A photographing protocol and image database. Appetite, 2016, 96, 166-173.	3.7	124
20	Effects of early nutrition and growth on brain volumes, white matter microstructure, and neurodevelopmental outcome in preterm newborns. Pediatric Research, 2018, 83, 102-110.	2.3	118
21	Brain Volumes at Term-Equivalent Age in Preterm Infants: Imaging Biomarkers for Neurodevelopmental Outcome through Early School Age. Journal of Pediatrics, 2016, 172, 88-95.	1.8	102
22	The Gaussian scale-space paradigm and the multiscale local jet. International Journal of Computer Vision, 1996, 18, 61-75.	15.6	94
23	ConvNet-Based Localization of Anatomical Structures in 3-D Medical Images. IEEE Transactions on Medical Imaging, 2017, 36, 1470-1481.	8.9	94
24	Automated Coronary Artery Calcification Scoring in Non-Gated Chest CT: Agreement and Reliability. PLoS ONE, 2014, 9, e91239.	2.5	90
25	Evaluation of automatic neonatal brain segmentation algorithms: The NeoBrainS12 challenge. Medical Image Analysis, 2015, 20, 135-151.	11.6	85
26	Robustness of Automated Methods for Brain Volume Measurements across Different MRI Field Strengths. PLoS ONE, 2016, 11, e0165719.	2.5	83
27	Deep learning–based MRâ€toâ€CT synthesis: The influence of varying gradient echo–based MR images as input channels. Magnetic Resonance in Medicine, 2020, 83, 1429-1441.	3.0	77
28	Deep learning analysis of left ventricular myocardium in CT angiographic intermediate-degree coronary stenosis improves the diagnostic accuracy for identification of functionally significant stenosis. European Radiology, 2019, 29, 2350-2359.	4.5	73
29	Automatic segmentation of MR brain images of preterm infants using supervised classification. NeuroImage, 2015, 118, 628-641.	4.2	71
30	What you see is what you eat: An ALE meta-analysis of the neural correlates of food viewing in children and adolescents. NeuroImage, 2015, 104, 35-43.	4.2	70
31	Deep Learning-Based Regression and Classification for Automatic Landmark Localization in Medical Images. IEEE Transactions on Medical Imaging, 2020, 39, 4011-4022.	8.9	70
32	Microstructural brain development between 30 and 40 weeks corrected age in a longitudinal cohort of extremely preterm infants. NeuroImage, 2014, 103, 214-224.	4.2	65
33	Dual matrix ordered subsets reconstruction for accelerated 3D scatter compensation in single-photon emission tomography. European Journal of Nuclear Medicine and Molecular Imaging, 1997, 25, 8-18.	6.4	63
34	An evaluation of automatic coronary artery calcium scoring methods with cardiac CT using the orCaScore framework. Medical Physics, 2016, 43, 2361-2373.	3.0	63
35	Development of Cortical Morphology Evaluated with Longitudinal MR Brain Images of Preterm Infants. PLoS ONE, 2015, 10, e0131552.	2.5	60
36	Cohort Profile: Cohort Hip and Cohort Knee (CHECK) study. International Journal of Epidemiology, 2016, 45, 36-44.	1.9	59

#	Article	IF	CITATIONS
37	Automatic Segmentation of Eight Tissue Classes in Neonatal Brain MRI. PLoS ONE, 2013, 8, e81895.	2.5	59
38	Relation between clinical risk factors, early cortical changes, and neurodevelopmental outcome in preterm infants. NeuroImage, 2016, 142, 301-310.	4.2	58
39	Developmental differences in the brain response to unhealthy food cues: an fMRI study of children and adults. American Journal of Clinical Nutrition, 2016, 104, 1515-1522.	4.7	57
40	Effects of Posthemorrhagic Ventricular Dilatation in the Preterm InfantÂonÂBrain Volumes and White Matter Diffusion Variables atÂTerm-Equivalent Age. Journal of Pediatrics, 2016, 168, 41-49.e1.	1.8	51
41	Automatic classification of focal liver lesions based on MRI and risk factors. PLoS ONE, 2019, 14, e0217053.	2.5	47
42	Deep Learning Analysis of Coronary Arteries in Cardiac CT Angiography for Detection of Patients Requiring Invasive Coronary Angiography. IEEE Transactions on Medical Imaging, 2020, 39, 1545-1557.	8.9	43
43	Placement of an inferior vena cava filter in a pig guided by high-resolution MR fluoroscopy at 1.5 T. Journal of Magnetic Resonance Imaging, 2000, 12, 599-605.	3.4	42
44	Automated remote fall detection using impact features from video and audio. Journal of Biomechanics, 2019, 88, 25-32.	2.1	41
45	Selective contrast-enhanced MR angiography. Magnetic Resonance in Medicine, 2000, 44, 575-582.	3.0	39
46	Scale Space Hierarchy. Journal of Mathematical Imaging and Vision, 2003, 18, 169-189.	1.3	39
47	Quantification of confounding factors in MRI-based dose calculations as applied to prostate IMRT. Physics in Medicine and Biology, 2017, 62, 948-965.	3.0	39
48	White matter hyperintensity shape and location feature analysis on brain MRI; proof of principle study in patients with diabetes. Scientific Reports, 2018, 8, 1893.	3.3	39
49	Radiogenomic Analysis of Breast Cancer by Linking MRI Phenotypes with Tumor Gene Expression. Radiology, 2020, 296, 277-287.	7.3	37
50	Functional MRI of Challenging Food Choices: Forced Choice between Equally Liked High- and Low-Calorie Foods in the Absence of Hunger. PLoS ONE, 2015, 10, e0131727.	2.5	37
51	Taste matters – effects of bypassing oral stimulation on hormone and appetite responses. Physiology and Behavior, 2014, 137, 9-17.	2.1	36
52	Dilated Convolutional Neural Networks for Cardiovascular MR Segmentation in Congenital Heart Disease. Lecture Notes in Computer Science, 2017, , 95-102.	1.3	36
53	White matter maturation in the neonatal brain is predictive of school age cognitive capacities in children born very preterm. Developmental Medicine and Child Neurology, 2017, 59, 939-946.	2.1	36
54	Accelerated SPECT image reconstruction with FBP and an image enhancement convolutional neural network. EJNMMI Physics, 2019, 6, 14.	2.7	34

#	Article	IF	CITATIONS
55	Subtypes of trait impulsivity differentially correlate with neural responses to food choices. Behavioural Brain Research, 2016, 296, 442-450.	2.2	32
56	The adverse effect of gradient nonlinearities on diffusion MRI: From voxels to group studies. NeuroImage, 2020, 205, 116127.	4.2	32
57	Automatic Quantification of Radiographic Finger Joint Space Width of Patients With Early Rheumatoid Arthritis. IEEE Transactions on Biomedical Engineering, 2016, 63, 2177-2186.	4.2	31
58	Evaluation of Variable Density and Data-Driven K-Space Undersampling for Compressed Sensing Magnetic Resonance Imaging. Investigative Radiology, 2016, 51, 410-419.	6.2	29
59	Impact of respiratory motion and acquisition settings on <scp>SPECT</scp> liver dosimetry for radioembolization. Medical Physics, 2017, 44, 5270-5279.	3.0	29
60	Deep learning from dualâ€energy information for wholeâ€heart segmentation in dualâ€energy and singleâ€energy nonâ€contrastâ€enhanced cardiac CT. Medical Physics, 2020, 47, 5048-5060.	3.0	29
61	The Sum of Its Parts—Effects of Gastric Distention, Nutrient Content and Sensory Stimulation on Brain Activation. PLoS ONE, 2014, 9, e90872.	2.5	28
62	Quality of MR thermometry during palliative MR-guided high-intensity focused ultrasound (MR-HIFU) treatment of bone metastases. Journal of Therapeutic Ultrasound, 2015, 3, 5.	2.2	28
63	Quantifying cardiacâ€induced brain tissue expansion using DENSE. NMR in Biomedicine, 2019, 32, e4050.	2.8	28
64	Quantification of deep medullary veins at 7 T brain MRI. European Radiology, 2016, 26, 3412-3418.	4.5	27
65	Trade-off between angular and spatial resolutions in in vivo fiber tractography. NeuroImage, 2016, 129, 117-132.	4.2	27
66	MRIâ€based synthetic CT shows equivalence to conventional CT for the morphological assessment of the hip joint. Journal of Orthopaedic Research, 2022, 40, 954-964.	2.3	27
67	Computed tomography perfusion evaluation after extracranial–intracranial bypass surgery. Clinical Neurology and Neurosurgery, 2015, 136, 139-146.	1.4	25
68	Prediction of cognitive and motor outcome of preterm infants based on automatic quantitative descriptors from neonatal MR brain images. Scientific Reports, 2017, 7, 2163.	3.3	25
69	Sex Differences in Coronary Artery and Thoracic Aorta Calcification and Their Association With Cardiovascular Mortality in Heavy Smokers. JACC: Cardiovascular Imaging, 2019, 12, 1808-1817.	5.3	25
70	Diffusion tensor imaging of the auditory nerve in patients with long-term single-sided deafness. Hearing Research, 2015, 323, 1-8.	2.0	24
71	Influence of water and fat heterogeneity on fatâ€referenced MR thermometry. Magnetic Resonance in Medicine, 2016, 75, 1187-1197.	3.0	24
72	DIRBoost–An algorithm for boosting deformable image registration: Application to lung CT intra-subject registration. Medical Image Analysis, 2014, 18, 449-459.	11.6	23

#	Article	IF	CITATIONS
73	Anterior-posterior length discrepancy of the spinal column in adolescent idiopathic scoliosis—a 3D CT study. Spine Journal, 2018, 18, 2259-2265.	1.3	23
74	Coronary calcium scoring with partial volume correction in anthropomorphic thorax phantom and screening chest CT images. PLoS ONE, 2018, 13, e0209318.	2.5	23
75	Computer-Aided Diagnosis in Multiparametric Magnetic Resonance Imaging Screening of Women With Extremely Dense Breasts to Reduce False-Positive Diagnoses. Investigative Radiology, 2020, 55, 438-444.	6.2	23
76	The Superoanterior Fasciculus (SAF): A Novel White Matter Pathway in the Human Brain?. Frontiers in Neuroanatomy, 2019, 13, 24.	1.7	22
77	MRA of hemodialysis access grafts and fistulae using selective contrast injection and flow interruption. Magnetic Resonance in Medicine, 2001, 45, 557-561.	3.0	21
78	Considering healthiness promotes healthier choices but modulates medial prefrontal cortex differently in children compared with adults. NeuroImage, 2017, 159, 325-333.	4.2	21
79	Development and body mass inversely affect children's brain activation in dorsolateral prefrontal cortex during food choice. Neurolmage, 2019, 201, 116016.	4.2	21
80	Validating faster DENSE measurements of cardiac-induced brain tissue expansion as a potential tool for investigating cerebral microvascular pulsations. NeuroImage, 2020, 208, 116466.	4.2	21
81	Comparison of the Biograph Vision and Biograph mCT for quantitative 90Y PET/CT imaging for radioembolisation. EJNMMI Physics, 2020, 7, 14.	2.7	21
82	Background suppression using magnetization preparation for contrast-enhanced MR projection angiography. Magnetic Resonance in Medicine, 2001, 46, 78-87.	3.0	20
83	Automated characterization of noise distributions in diffusion MRI data. Medical Image Analysis, 2020, 65, 101758.	11.6	20
84	Liver segmentation and metastases detection in MR images using convolutional neural networks. Journal of Medical Imaging, 2019, 6, 1.	1.5	20
85	Toward Simultaneous Real-Time Fluoroscopic and Nuclear Imaging in the Intervention Room. Radiology, 2016, 278, 232-238.	7.3	19
86	Automatic Localization of Cochlear Implant Electrode Contacts in CT. Ear and Hearing, 2017, 38, e376-e384.	2.1	19
87	Complementary Value of Contralateral Parenchymal Enhancement on DCE-MRI to Prognostic Models and Molecular Assays in High-risk ER+/HER2â^' Breast Cancer. Clinical Cancer Research, 2017, 23, 6505-6515.	7.0	18
88	CT perfusion analysis by nonlinear regression for predicting hemorrhagic transformation in ischemic stroke. Medical Physics, 2015, 42, 4610-4618.	3.0	17
89	Serum Lipid Levels, Body Mass Index, and Their Role in Coronary Artery Calcification. Circulation: Cardiovascular Genetics, 2015, 8, 327-333.	5.1	17
90	Sheet Probability Index (SPI): Characterizing the geometrical organization of the white matter with diffusion MRI. NeuroImage, 2016, 142, 260-279.	4.2	17

#	Article	IF	CITATIONS
91	In Vivo Molecular MRI of ICAM-1 Expression on Endothelium and Leukocytes from Subacute to Chronic Stages After Experimental Stroke. Translational Stroke Research, 2017, 8, 440-448.	4.2	17
92	Fast technetiumâ€99m liver <scp>SPECT</scp> for evaluation of the pretreatment procedure for radioembolization dosimetry. Medical Physics, 2019, 46, 345-355.	3.0	17
93	Radioembolization lung shunt estimation based on a <sup>90</sup> Y pretreatment procedure: A phantom study. Medical Physics, 2018, 45, 4744-4753.	3.0	16
94	Generalized Richardson-Lucy (GRL) for analyzing multi-shell diffusion MRI data. NeuroImage, 2020, 218, 116948.	4.2	16
95	Linear Scale-Space Theory from Physical Principles. Journal of Mathematical Imaging and Vision, 1998, 9, 103-139.	1.3	15
96	Quantifying the brain's sheet structure with normalized convolution. Medical Image Analysis, 2017, 39, 162-177.	11.6	15
97	Fast Fourierâ€based simulation of offâ€resonance artifacts in steadyâ€state gradient echo MRI applied to metal object localization. Magnetic Resonance in Medicine, 2017, 78, 2035-2041.	3.0	15
98	A Dual-layer Detector for Simultaneous Fluoroscopic and Nuclear Imaging. Radiology, 2019, 290, 833-838.	7.3	15
99	Seeing More by Showing Less: Orientation-Dependent Transparency Rendering for Fiber Tractography Visualization. PLoS ONE, 2015, 10, e0139434.	2.5	14
100	Fast nonlinear regression method for CT brain perfusion analysis. Journal of Medical Imaging, 2016, 3, 026003.	1.5	14
101	DCE-MRI and IVIM-MRI of rabbit Vx2 tumors treated with MR-HIFU-induced mild hyperthermia. Journal of Therapeutic Ultrasound, 2016, 4, 9.	2.2	14
102	Automatic quantification of ischemic injury on diffusion-weighted MRI of neonatal hypoxic ischemic encephalopathy. NeuroImage: Clinical, 2017, 14, 222-232.	2.7	14
103	Harmonization of diffusion <scp>MRI</scp> data sets with adaptive dictionary learning. Human Brain Mapping, 2020, 41, 4478-4499.	3.6	14
104	<sup>19</sup> F MRSI of capecitabine in the liver at 7 T using broadband transmit–receive antennas a dualâ€band RF pulses. NMR in Biomedicine, 2015, 28, 1433-1442.	and 2.8	13
105	Feasibility of imaging <sup>90</sup> Y microspheres at diagnostic activity levels for hepatic radioembolization treatment planning. Medical Physics, 2020, 47, 1105-1114.	3.0	13
106	The effect of gradient nonlinearities on fiber orientation estimates from spherical deconvolution of diffusion magnetic resonance imaging data. Human Brain Mapping, 2021, 42, 367-383.	3.6	13
107	Fast quantitative reconstruction with focusing collimators for liver SPECT. EJNMMI Physics, 2018, 5, 28.	2.7	12
108	Development and Testing of a Magnetic Resonance (MR) Conditional Afterloader for Source Tracking in Magnetic Resonance Imaging-Guided High-Dose-Rate (HDR) Brachytherapy. International Journal of Radiation Oncology Biology Physics, 2018, 102, 960-968.	0.8	12

#	Article	IF	CITATIONS
109	Effect of prolonged acquisition intervals for CTâ€perfusion analysis methods in patients with ischemic stroke. Medical Physics, 2019, 46, 3156-3164.	3.0	12
110	Preventive and Abortive Strategies for Stimulation Based Control of Epilepsy: A Computational Model Study. International Journal of Neural Systems, 2016, 26, 1650028.	5.2	11
111	Subject-specific four-dimensional liver motion modeling based on registration of dynamic MRI. Journal of Medical Imaging, 2016, 3, 1.	1.5	11
112	Automatic joint detection in rheumatoid arthritis hand radiographs. , 2013, , .		10
113	Influence of Thin Slice Reconstruction on CT Brain Perfusion Analysis. PLoS ONE, 2015, 10, e0137766.	2.5	10
114	Challenges in <scp>MR</scp> â€only seed localization for postimplant dosimetry in permanent prostate brachytherapy. Medical Physics, 2017, 44, 5051-5060.	3.0	10
115	Reducing variability in along-tract analysis with diffusion profile realignment. NeuroImage, 2019, 199, 663-679.	4.2	10
116	Respiratory motion compensation in interventional liver SPECT using simultaneous fluoroscopic and nuclear imaging. Medical Physics, 2019, 46, 3496-3507.	3.0	10
117	Performance of a dual-layer scanner for hybrid SPECT/CBCT. Physics in Medicine and Biology, 2019, 64, 105020.	3.0	10
118	Are contralateral parenchymal enhancement on dynamic contrast-enhanced MRI and genomic ER-pathway activity in ER-positive/HER2-negative breast cancer related?. European Journal of Radiology, 2019, 121, 108705.	2.6	9
119	Al-Based Quantification of Planned Radiation Therapy Dose to Cardiac Structures and Coronary Arteries in Patients With Breast Cancer. International Journal of Radiation Oncology Biology Physics, 2022, 112, 611-620.	0.8	9
120	Al-Based Radiation Dose Quantification for Estimation of Heart Disease Risk in Breast Cancer Survivors After Radiation Therapy. International Journal of Radiation Oncology Biology Physics, 2022, 112, 621-632.	0.8	9
121	Synthetic CT for the planning of MR-HIFU treatment of bone metastases in pelvic and femoral bones: a feasibility study. European Radiology, 2022, , 1.	4.5	9
122	Differential and Integral Geometry of Linear Scale-Spaces. Journal of Mathematical Imaging and Vision, 1998, 9, 5-27.	1.3	8
123	Registration of organs with sliding interfaces and changing topologies. Proceedings of SPIE, 2014, , .	0.8	8
124	Simultaneous fluoroscopic and nuclear imaging: impact of collimator choice on nuclear image quality. Medical Physics, 2017, 44, 249-261.	3.0	8
125	CT-based study of vertebral and intravertebral rotation in right thoracic adolescent idiopathic scoliosis. European Spine Journal, 2019, 28, 3044-3052.	2.2	8
126	Deep learning-based whole-heart segmentation in 4D contrast-enhanced cardiac CT. Computers in Biology and Medicine, 2022, 142, 105191.	7.0	8

Max A Viergever

#	Article	IF	CITATIONS
127	Interactive lung segmentation in abnormal human and animal chest CT scans. Medical Physics, 2014, 41, 081915.	3.0	7
128	Semi-automatic classification of textures in thoracic CT scans. Physics in Medicine and Biology, 2016, 61, 5906-5924.	3.0	6
129	Automatic Quantification of Radiographic Wrist Joint Space Width of Patients With Rheumatoid Arthritis. IEEE Transactions on Biomedical Engineering, 2017, 64, 2695-2703.	4.2	6
130	Implications of Extracranial Distortion in Ultra-High-Field Magnetic Resonance Imaging for Image-Guided Cranial Neurosurgery. World Neurosurgery, 2019, 126, e250-e258.	1.3	6
131	A computed tomography-based spatial reference for pedicle screw placement in adolescent idiopathic scoliosis. Spine Deformity, 2020, 8, 67-76.	1.5	6
132	Impact of automatically detected motion artifacts on coronary calcium scoring in chest computed tomography. Journal of Medical Imaging, 2018, 5, 1.	1.5	6
133	Efficient cascaded Vâ€net optimization for lower extremity CT segmentation validated using bone morphology assessment. Journal of Orthopaedic Research, 2022, , .	2.3	6
134	Linearised Euclidean Shortening Flow of Curve Geometry. International Journal of Computer Vision, 1999, 34, 29-67.	15.6	5
135	On-line flow quantification by low-resolution phase-contrast MR imaging and model-based postprocessing. Journal of Magnetic Resonance Imaging, 2000, 12, 623-631.	3.4	5
136	A Dynamic Scale–Space Paradigm. Journal of Mathematical Imaging and Vision, 2001, 15, 127-168.	1.3	5
137	Subject-specific liver motion modeling in MRI: a feasibility study on spatiotemporal prediction. Physics in Medicine and Biology, 2017, 62, 2581-2597.	3.0	5
138	Fast and accurate quantitative determination of the lung shunt fraction in hepatic radioembolization. Physics in Medicine and Biology, 2019, 64, 235002.	3.0	5
139	CT to MR registration of complex deformations in the knee joint through dual quaternion interpolation of rigid transforms. Physics in Medicine and Biology, 2021, 66, 175024.	3.0	5
140	Placement of an inferior vena cava filter in a pig guided by highâ€resolution MR fluoroscopy at 1.5 T. Journal of Magnetic Resonance Imaging, 2000, 12, 599-605.	3.4	5
141	Microstructural White Matter Tissue Characteristics Are Modulated by Homocysteine: A Diffusion Tensor Imaging Study. PLoS ONE, 2015, 10, e0116330.	2.5	5
142	fMRI based BCI control using spatial visual attention at 7T. , 2009, , .		4
143	Detecting cerebral microbleeds in 7.0 T MR images using the radial symmetry transform. , 2011, , .		4
144	Corrections to "Breast cancer histopathology image analysis: A review―[May 14 1400-1411]. IEEE Transactions on Biomedical Engineering, 2014, 61, 2819-2819.	4.2	4

#	Article	IF	CITATIONS
145	Atlas-Based Mosaicing of Left Atrial 3-D Transesophageal Echocardiography Images. Ultrasound in Medicine and Biology, 2017, 43, 765-774.	1.5	4
146	Benchmarking Distance Control and Virtual Drilling for Lateral Skull Base Surgery. World Neurosurgery, 2018, 109, e217-e228.	1.3	4
147	MRI artifact simulation for clinically relevant MRI sequences for guidance of prostate HDR brachytherapy. Physics in Medicine and Biology, 2019, 64, 095006.	3.0	4
148	Fiber orientation distribution from diffusion MRI: Effects of inaccurate response function calibration. Journal of Neuroimaging, 2021, 31, 1082-1098.	2.0	4
149	Enforcing stochastic inverse consistency in non-rigid image registration and matching. , 2008, , .		3
150	Classification of coronary artery calcifications according to motion artifacts in chest CT using a convolutional neural network. Proceedings of SPIE, 2017, , .	0.8	3
151	SMART tracking: Simultaneous anatomical imaging and real-time passive device tracking for MR-guided interventions. Physica Medica, 2019, 64, 252-260.	0.7	3
152	Early detection of small volume stroke and thromboembolic sources with computed tomography: Rationale and design of the ENCLOSE study. European Stroke Journal, 2020, 5, 432-440.	5.5	3
153	Optimization of Parallel-Hole Collimators for Intraoperative Localization of Iodine-125 Seeds. IEEE Transactions on Nuclear Science, 2016, 63, 2527-2532.	2.0	2
154	Estimation of lung shunt fraction from simultaneous fluoroscopic and nuclear images. Physics in Medicine and Biology, 2017, 62, 8210-8225.	3.0	2
155	Automatic, Fast and Robust Characterization of Noise Distributions for Diffusion MRI. Lecture Notes in Computer Science, 2018, , 304-312.	1.3	2
156	Distance Control and Virtual Drilling Improves Anatomical Orientation During Anterior Petrosectomy. Operative Neurosurgery, 2020, 18, 83-91.	0.8	2
157	Synchronous Breast Cancer: Phenotypic Similarities on MRI. Journal of Magnetic Resonance Imaging, 2020, 51, 1858-1867.	3.4	2
158	Rapid 2D variable flip angle method for accurate and precise T 1 measurements over a wide range of T 1 Âvalues. NMR in Biomedicine, 2021, 34, e4542.	2.8	2
159	Interleaved water and fat MR thermometry for monitoring high intensity focused ultrasound ablation of bone lesions. Magnetic Resonance in Medicine, 2021, 86, 2647-2655.	3.0	2
160	Implicit surface registration with surface-oriented anisotropic deformation field smoothing. , 2013, , .		1
161	Detecting cortical cerebral microinfarcts in 7.0 T MR images. , 2013, , .		1
162	Atlas-based mosaicing of 3D transesophageal echocardiography images of the left atrium. , 2015, , .		1

#	Article	IF	CITATIONS
163	Region based perfusion estimation in peripherals using C-arm systems: A simulation study. , 2011, , .		0
164	Optimization Strategies for Interactive Classification of Interstitial Lung Disease Textures. Frontiers in ICT, 2016, 3, .	3.6	0
165	Short and long time MR signal behavior of randomly distributed water and fat—numerical simulations. NMR in Biomedicine, 2016, 29, 1634-1643.	2.8	0
166	Selection Strategies for Atlas-Based Mosaicing of Left Atrial 3-D Transesophageal Echocardiography Data. Ultrasound in Medicine and Biology, 2018, 44, 1533-1543.	1.5	0
167	System for imageâ€guided resection of nonpalpable breast lesions: Proof of concept. Medical Physics, 2018, 45, 2169-2178.	3.0	0
168	isoPhasor: a generic and precise marker visualization, localization, and quantification method based on phase saddles in 3D MR imaging. Magnetic Resonance in Medicine, 2019, 81, 2038-2051.	3.0	0